# PET Imaging of Very Late Antigen-4 in Melanoma: Comparison of $^{68}$Ga- and $^{64}$Cu-Labeled NODAGA and CB-TE1A1P-LLP2A Conjugates

Wissam Beaino[1] and Carolyn J. Anderson[1–3]

*[1]Department of Radiology, University of Pittsburgh, Pittsburgh, Pennsylvania; [2]Department of Pharmacology and Chemical Biology, University of Pittsburgh, Pittsburgh, Pennsylvania; and [3]Department of Bioengineering, University of Pittsburgh, Pittsburgh, Pennsylvania*

Melanoma is a malignant tumor derived from epidermal melanocytes, and it is known for its aggressiveness, therapeutic resistance, and predisposition for late metastasis. Very late antigen-4 (VLA-4; also called integrin $\alpha_4\beta_1$) is a transmembrane noncovalent heterodimer overexpressed in melanoma tumors that plays an important role in tumor growth, angiogenesis, and metastasis by promoting adhesion and migration of cancer cells. In this study, we evaluated 2 conjugates of a high-affinity VLA-4 peptidomimetic ligand, LLP2A, for PET/CT imaging in a subcutaneous and metastatic melanoma tumor. **Methods:** LLP2A was conjugated to 1,4,8,11-tetraazacyclotetradecane-1-(methane phosphonic acid)-8-(methane carboxylic acid) (CB-TE1A1P) and 2-(4,7-bis(carboxymethyl)-1,4,7-triazonan-1-yl)pentanedioic acid (NODAGA) chelators for $^{68}$Ga and $^{64}$Cu labeling. The conjugates were synthesized by solid-phase peptide synthesis, purified by reversed-phase high-performance liquid chromatography, and verified by liquid chromatography mass spectrometry. Saturation and competitive binding assays with B16F10 melanoma cells determined the affinity of the compounds for VLA-4. The biodistributions of the LLP2A conjugates were evaluated in murine B16F10 subcutaneous tumor–bearing C57BL/6 mice. Melanoma metastasis was induced by intracardiac injection of B16F10 cells. PET/CT imaging was performed at 2, 4, and 24 h after injection for the $^{64}$Cu tracers and 1 h after injection for the $^{68}$Ga tracer. **Results:** $^{64}$Cu-labeled CB-TE1A1P-PEG$_4$-LLP2A and NODAGA-PEG$_4$-LLP2A showed high affinity to VLA-4, with a comparable dissociation constant (0.28 vs. 0.23 nM) and receptor concentration (296 vs. 243 fmol/mg). The tumor uptake at 2 h after injection was comparable for the 2 probes, but $^{64}$Cu-CB-TE1A1P-PEG$_4$-LLP2A trended toward higher uptake than $^{64}$Cu-NODAGA-PEG$_4$-LLP2A (16.9 ± 2.2 vs. 13.4 ± 1.7 percentage injected dose per gram, $P = 0.07$). Tumor-to-muscle and tumor-to-blood ratios from biodistribution and PET/CT images were significantly higher for $^{64}$Cu-CB-TE1A1P-PEG$_4$-LLP2A than $^{64}$Cu-NODAGA-PEG$_4$-LLP2A (all $P$ values $< 0.05$). PET/CT imaging of metastatic melanoma with $^{68}$Ga-NODAGA-PEG$_4$-LLP2A and $^{64}$Cu-NODAGA-PEG$_4$-LLP2A showed high uptake of the probes at the site of metastasis, correlating with the bioluminescence imaging of the tumor. **Conclusion:** These data demonstrate that $^{64}$Cu-labeled CB-TE1A1P/NODAGA LLP2A conjugates and $^{68}$Ga-labeled NODAGA-LLP2A are excellent imaging agents for melanoma and potentially other VLA-4–positive tumors. $^{64}$Cu-CB-TE1A1P-PEG$_4$-LLP2A had the most optimal tumor–to–nontarget tissue ratios for translation into humans as a PET imaging agent for melanoma.

**Key Words:** LLP2A; melanoma; VLA-4; PET; metastasis

**J Nucl Med 2014; 55:1856–1863**
DOI: 10.2967/jnumed.114.144881

Melanoma is the fifth most common cancer in the United States. It is a malignant tumor derived from epidermal melanocytes, and it is known for its therapeutic resistance, aggressive clinical behavior, and predisposition for late metastasis. Malignant melanoma primarily metastasizes to lymph nodes, lungs, bone, liver, brain, and adrenals glands (*1*). The incidence of melanoma has increased steadily and rapidly worldwide (*2,3*). Primary melanoma can be cured by surgical resection (*4*); however, despite significant advances in treating melanoma over the past 2 decades, long-term survival is still low, with a 5-y survival rate of less than 10% for people with distant metastasis.

There have been significant advances in the treatment of metastatic melanoma over the past decade. Targeted therapy using BRAF inhibitors has shown promising results, but most patients develop recurrence and relapse at a median of 6–7 mo (*5,6*). Early diagnosis and accurate staging of the disease is critical to increased survival. $^{18}$F-FDG PET has been established as an important tool and is currently the standard of care for staging melanoma because of its high sensitivity for detecting metastases and providing a 3-dimensional image that facilitates the surgical approach for metastatic lymph node resection (*7*). $^{18}$F-FDG is transported by the glucose 1 transporter and accumulates in tumor cells, but it is not specific for melanoma and can result in false-positive scans caused by secondary, inflammatory, or infectious processes; exercised skeletal muscle; or other benign etiologies (*8*). In addition, it has been reported that $^{18}$F-FDG often fails to detect metastatic lesions less than 1 cm (*7*).

More specific PET probes for imaging melanoma may have advantages for visualizing and monitoring the disease and may increase the detection of small metastasis. *N*-[2-(diethylamino) ethy1]-4-$^{18}$F-fluorobenzamide ($^{18}$F-FBZA), which targets melanin, was evaluated by Ren et al. (*9*) for imaging malignant melanoma and showed uptake comparable to $^{18}$F-FDG. Guo et al. (*10*) used a SPECT probe, $^{67}$Ga-DOTA-GlyGlu-CycMSH, for specific imaging of melanoma and metastasis in a B16F10 mouse model. Beer et al. (*11*) evaluated the biodistribution

Received Jun. 24, 2014; revision accepted Aug. 8, 2014.
For correspondence or reprints contact: Carolyn J. Anderson, Department of Radiology, University of Pittsburgh, 100 Technology Dr., Suite 452, Pittsburgh, PA 15219.
E-mail: andersoncj@upmc.edu
Published online Sep. 25, 2014.

and pharmacokinetics of $^{18}$F-galacto-RGD (arginine, glycine, aspartic acid) in humans for PET imaging of malignant melanoma and other $\alpha_v\beta_3$-positive tumors; however, there was inconsistent uptake of this tracer in the metastatic melanoma lesions.

In the past several years, there has been increasing interest in targeting very late antigen-4 (VLA-4; also called integrin $\alpha_4\beta_1$) for cancer imaging and therapy. VLA-4 is a transmembrane noncovalent heterodimer expressed in cancers such as melanoma, multiple myeloma, and lymphoma and plays an important role in tumor growth, angiogenesis, and metastasis by promoting adhesion and migration of cancer cells (*12–14*). In human melanoma, studies have shown that increased expression of the VLA-4 integrin correlates with tumor progression and development of metastasis (*15–19*).

A high-affinity peptidomimetic ligand (LLP2A) for VLA-4 was identified from a 1-bead 1-compound library (*20*). $^{111}$In-labeled DOTA-LLP2A and $^{64}$Cu-labeled 11-bis(carboxymethyl)-1,4,8,11-tetraazabicyclo[6.6.2] hexadecane-LLP2A (CB-TE2A-LLP2A) were compared for SPECT and PET imaging of Raji B-cell lymphoma xenografts, in which they showed uptake in the tumor as well in the VLA-4–expressing organs (spleen, bone marrow). $^{64}$Cu-labeled CB-TE2A-LLP2A was also evaluated for imaging the VLA-4–positive bone marrow–derived cells, putatively the premetastatic niche, in a breast cancer bone metastasis model (*21*). In the same study, the biodistribution of $^{64}$Cu-CB-TE2A-LLP2A in mice bearing subcutaneous B16F10 melanoma tumors was reported, demonstrating specific tumor uptake with a relatively high tumor-to-blood ratio. LLP2A was also conjugated to a second-generation cross-bridge chelator, 1,4,8,11-tetraazacyclotetradecane-1-(methane phosphonic acid)-8-(methane carboxylic acid) (CB-TE1A1P), for $^{64}$Cu labeling, and this new conjugate had significantly higher tumor uptake and better tumor-to-nontumor ratios than $^{64}$Cu-CB-TE2A-LLP2A, as well as more rapid clearance from nontarget tissues (*22*). $^{64}$Cu-CB-TE1A1P-LLP2A also showed high uptake in multiple myeloma tumors in mice (*23*).

$^{68}$Ga (half-life, 68 min; $\beta^+$,1.92 MeV, 89%) is readily available on-site at a relatively low cost from a $^{68}$Ge/$^{68}$Ga generator. $^{64}$Cu (half-life, 12.7 h) is produced on a cyclotron, and the longer half-life makes it suitable for imaging at longer time points, which enhances tumor–to–nontarget tissue contrast. Both radionuclides have the potential for routine clinical use. In this study, we evaluated and compared the 2-(4,7-bis(carboxymethyl)-1,4,7-triazonan-1-yl)pentanedioic acid (NODAGA) and the CB-TE1A1P chelators conjugated to LLP2A peptidomimetic with a $PEG_4$ linker between the chelator and peptidomimetic. The conjugates were labeled with $^{68}$Ga or $^{64}$Cu, and their affinity and internalization were evaluated in vitro using B16F10 melanoma cell lines and in vivo for PET/CT imaging in a B16F10 melanoma subcutaneous tumor and melanoma metastasis to demonstrate the potential for translation to humans with metastatic melanoma.

## MATERIALS AND METHODS

Additional materials and methods sections, including reagents, synthesis of NODAGA-$PEG_4$-LLP2A and CB-TE1A1P-$PEG_4$-LLP2A, radiolabeling of NODAGA-$PEG_4$-LLP2A and CB-TE1A1P-$PEG_4$-LLP2A with $^{64}$Cu, radiolabeling of NODAGA-$PEG_4$-LLP2A with $^{68}$Ga, stability and serum protein binding, cell studies, internalization assay, animal model, and bioluminescence imaging, are provided in the supplemental materials (available at http://jnm.snmjournals.org).

### Binding Assay

Cell experiments were performed to determine the binding affinity of $^{64}$Cu-NODAGA-$PEG_4$-LLP2A and $^{64}$Cu-CB-TE1A1P-$PEG_4$-LLP2A in VLA-4–positive B16F10 mouse melanoma cells. Cells were seeded in 24-well plates (100,000 cells per well) 24 h before the experiment. Before the experiment, cells were washed twice with 1 mL of Hanks balanced salt solution (HBSS), and 0.5 mL of binding medium (HBSS with 0.1% bovine serum albumin and 1 mM $Mn^{2+}$) was added to each well. Then 15 μg of LLP2A-$PEG_4$ were added to half of the wells as cold block to determine in vitro nonspecific binding, followed by 1 of the $^{64}$Cu-labeled tracers in increasing concentrations (0.2–30 nM). The samples were incubated for 3 h on ice. After incubation, the radioactive medium was removed. Cell pellets were rinsed twice with ice-cold binding buffer (1 mL) and dissolved in 0.5% sodium dodecyl sulfate solution. The radioactivity in each fraction was measured in a well counter (Cobra II γ counter; Packard). The protein content of each cell lysate sample was determined (BCA Protein Assay Kit; Pierce). The measured radioactivity associated with the cells was normalized to the amount of cell protein present (cpm/mg of protein). The dissociation constant ($K_d$) and receptor concentration ($B_{max}$) were calculated using PRISM 5 software (GraphPad).

The competitive binding assay was performed to determine the binding affinity of gallium-NODAGA-$PEG_4$-LLP2A by competition with $^{64}$Cu-NODAGA-$PEG_4$-LLP2A in VLA-4–positive B16F10 mouse melanoma cells. NODAGA-$PEG_4$-LLP2A was labeled with an excess of cold gallium (100-fold) under the same conditions as $^{68}$Ga (pH 4, 70°C, 20 min). Cells were seeded in 24-well plates (100,000 cells per well) 24 h before the experiment. Before the experiment, cells were washed twice with 1 mL of HBSS. Then different mixtures of $^{64}$Cu-NODAGA-$PEG_4$-LLP2A (1.1 nM) and increasing concentrations of gallium-NODAGA-$PEG_4$-LLP2A (0.005, 0.015, 0.05, 0.15, 0.5, 1.5, 5, 50, 500, 5,000, and 50,000 nM) in 0.5 mL of binding medium (HBSS with 0.1% bovine serum albumin and 1 mM $Mn^{2+}$) were added to each well in quadruplicate. The samples were incubated for 3 h on ice. After incubation, the radioactive medium was removed. Cell pellets were rinsed with ice-cold binding buffer (1 mL) twice and dissolved in 0.5% sodium dodecyl sulfate. The radioactivity in each fraction was measured in a γ counter (Cobra II; Packard). The protein content of each cell lysate sample was determined (BCA Protein Assay Kit; Pierce). The measured radioactivity associated with the cells was normalized to the amount of cell protein present (cpm/mg of protein). The inhibitor constant ($K_i$) and the half maximal inhibitory concentration ($IC_{50}$) were calculated using PRISM 5.

### PET/CT Imaging and Analysis

All animal studies were conducted under a protocol approved by the University of Pittsburgh Institutional Animal Care and Use Committee. C57BL/6J xenograft tumor–bearing mice ($n$ = 6 per compound) were injected intravenously (lateral tail vein) with $^{68}$Ga-NODAGA-$PEG_4$-LLP2A (7.4 MBq, 370 ng), $^{64}$Cu-NODAGA-$PEG_4$-LLP2A (7.4 MBq, 200 ng), or $^{64}$Cu-CB-TE1A1P-$PEG_4$-LLP2A (7.4 MBq, 200 ng). Half of the mice received a dose that was premixed with LLP2A-$PEG_4$ (50 μg) for blocking. For $^{68}$Ga imaging, at 1 h after injection mice were anesthetized with 2% isoflurane, and small-animal PET/CT was performed. Static images were collected for 10 min using a small-animal Inveon PET/CT scanner (Siemens Medical Solution), with a tangential and radial full width at half maximum of 1.5 mm at the center of the field of view and 1.8 mm at the edge of the field of view. For $^{64}$Cu imaging, at 2, 4, and 24 h mice were anesthetized with 2% isoflurane, and small-animal PET/CT was performed. Static images were collected for 15 min. PET and CT images were coregistered with Inveon Research Workstation (IRW) software (Siemens Medical Solutions). PET images were reconstructed with the ordered-subsets expectation maximization 3-dimensional/maximum a posteriori probability

algorithm, and the analysis of images was done using IRW. Regions of interest were drawn using the CT scan, and the associated PET activities were calculated using the IRW software. Standardized uptake values (SUVs) were calculated by the IRW software based on the following formula: SUV = ([Bq/mL] × [animal weight (g)]/[injected dose (Bq)]).

### Biodistribution Experiments

B16F10 tumor–bearing C57BL/6 mice ($n$ = 4 per group) were injected intravenously with $^{68}$Ga-NODAGA-PEG$_4$-LLP2A (5.55 MBq, 277 ng) or $^{64}$Cu-NODAGA-PEG$_4$-LLP2A or $^{64}$Cu-CB-TE1A1P-LLP2A (2.8 MBq, 75 ng). The tumor-bearing mice were sacrificed at 1 h after injection for $^{68}$Ga biodistribution and 2 and 4 h for $^{64}$Cu biodistribution. The blood, heart, intestines, lungs, liver, spleen, kidneys, muscle, bone, thymus, and tumor were harvested, weighed, and counted in a γ counter. An additional group of mice was injected with $^{64}$Cu- or $^{68}$Ga-labeled radiopharmaceuticals premixed with 100 μg of LLP2A-PEG$_4$ to serve as a blocking agent and sacrificed at 1 or 2 h. The percentage injected dose per gram of tissue (%ID/g) was determined by decay correction for each sample normalized to a standard of known weight, which was representative of the injected dose.

### Statistical Analysis

All data are presented as mean ± SD. Groups were compared using 2-tailed Student $t$ test or 2-way ANOVA. $P$ values of less than 0.05 were considered statistically significant.

## RESULTS

### Radiochemistry and In Vitro studies

$^{68}$Ga- and $^{64}$Cu-LLP2A conjugates (Fig. 1) were radiolabeled in 30 min at 70°C in acetate buffer at a specific activity of 37 MBq/μg and in greater than 98% radiochemical purity. $^{64}$Cu-NODAGA-PEG$_4$-LLP2A and $^{64}$Cu-CB-TE1A1P-PEG$_4$-LLP2A were stable in human serum, and no free $^{64}$Cu or degradation products were detected after 28 h. At 2 and 4 h, more $^{64}$Cu-CB-TE1A1P-PEG$_4$-LLP2A than $^{64}$Cu-NODAGA-PEG$_4$-LLP2A bound to plasma proteins (2 and 4 h: 4.8% ± 0.1% and 5.1% ± 0.2%, respectively, for $^{64}$Cu-CB-TE1A1P-PEG$_4$-LLP2A; and 2.6% ± 0.2% and 2.9% ± 0.2%, respectively, for $^{64}$Cu-NODAGA-PEG$_4$-LLP2A) (Table 1).

### Cell Binding Assay

B16F10 mouse melanoma cells express high levels of VLA-4 (*22*). Representative saturation binding curves of $^{64}$Cu-CB-TE1A1P-PEG$_4$-LLP2A and $^{64}$Cu-NODAGA-PEG$_4$-LLP2A to B16F10 cells are shown in Supplemental Figures 4A and 4C, respectively. $^{68}$Ga has a short half-life (68 min) and is not suitable for the saturation binding assay conditions. Therefore, a competitive binding assay was performed to evaluate the $IC_{50}$ and $K_i$ of cold gallium-NODAGA-PEG$_4$-LLP2A. Cold gallium-NODAGA-PEG$_4$-LLP2A was competed with $^{64}$Cu-NODAGA-PEG$_4$-LLP2A in B16F10 cells at 4°C (Supplemental Fig. 4B). The saturation binding data show that $^{64}$Cu-CB-TE1A1P-PEG$_4$-LLP2A and $^{64}$Cu-NODAGA-PEG$_4$-LLP2A bind with similar affinity to VLA-4, with a $K_d$ of 0.28 ± 0.03 and 0.23 ± 0.03 nM, respectively. $^{64}$Cu-CB-TE1A1P-PEG$_4$-LLP2A has a higher $B_{max}$ (296 ± 4.5 fmol/mg) than $^{64}$Cu-NODAGA-PEG$_4$-LLP2A (243 ± 5.2 fmol/mg). Gallium-NODAGA-PEG$_4$-LLP2A binds with an affinity comparable to $^{64}$Cu-NODAGA-PEG$_4$-LLP2A, with an $IC_{50}$ of 0.68 (95% confidence interval, 0.53–0.86) and $K_i$ of 0.11 nM (95% confidence interval, 0.08–0.13) (Table 2).

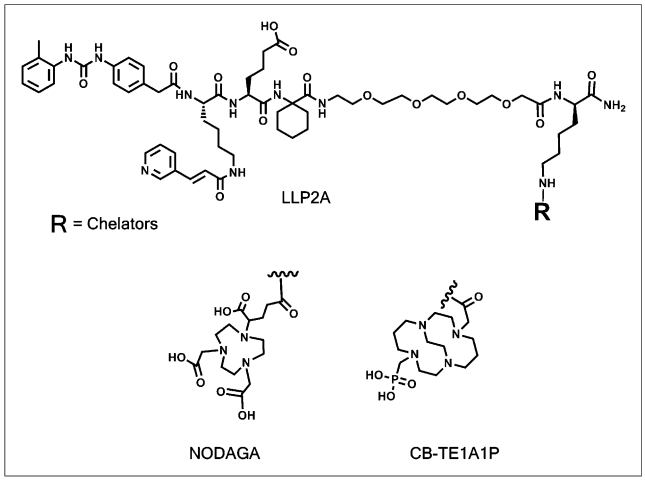


**FIGURE 1.** Structures of NODAGA-PEG$_4$-LLP2A and CB-TE1A1P-PEG$_4$-LLP2A.

**TABLE 1**
Amount (%) of LLP2A Conjugates Bound to Plasma Protein

| Time (h) | CB-TE1A1P | NODAGA |
|---|---|---|
| 2 | 4.8 ± 0.1 | 2.6 ± 0.2 |
| 4 | 5.1 ± 0.2 | 2.9 ± 0.2 |

$n$ = 3; values are expressed as mean ± SD.

### Internalization

The internalization of $^{64}$Cu-labeled NODAGA-PEG$_4$-LLP2A and CB-TE1A1P-PEG$_4$-LLP2A was evaluated in B16F10 melanoma cells (Fig. 2). The 2 compounds internalize rapidly (<15 min after addition), and the CB-TE1A1P analog internalized to a greater extent than the NODAGA compound (479.3 ± 27.5 vs. 304.9 ± 43.8 fmol/mg, respectively; $P < 0.01$). The internalization of $^{64}$Cu-CB-TE1A1P-PEG$_4$-LLP2A increased over time, whereas the internalization of $^{64}$Cu-NODAGA-PEG$_4$-LLP2A hit a plateau after 2 h. At 4 h, we see a significantly higher internalization of the CB-TE1A1P compound than of the NODAGA compound (1,024.1 ± 70.3 vs. 750.3 ± 70.1 fmol/mg, respectively; $P < 0.01$).

### Biodistribution of $^{64}$Cu- and $^{68}$Ga-LLP2A Conjugates

Mice were sacrificed at 2 and 4 h after administration of $^{64}$Cu-CB-TE1A1P-PEG$_4$-LLP2A or $^{64}$Cu-NODAGA-PEG$_4$-LLP2A (2.8 MBq, 37 MBq/μg) (Table 3). At 2 h, both agents showed comparable

**TABLE 2**
Binding Affinity of $^{64}$Cu-CB-TE1A1P-PEG$_4$-LLP2A, $^{64}$Cu-NODAGA-PEG$_4$-LLP2A, and Gallium-NODAGA-PEG$_4$-LLP2A

| Probe | $K_d$ (nM) | $B_{max}$ (fmol/mg) |
|---|---|---|
| $^{64}$Cu-CBTE1A1P-PEG$_4$-LLP2A | 0.28 ± 0.03 | 296 ± 4.5 |
| $^{64}$Cu-NODAGA-PEG$_4$-LLP2A | 0.23 ± 0.03 | 243 ± 5.1 |
| | $IC_{50}$ (nM) | Ki (nM) |
| Gallium-NODAGA-PEG$_4$-LLP2A | 0.67 | 0.11 |

$n$ = 3; values are expressed as mean ± SE.

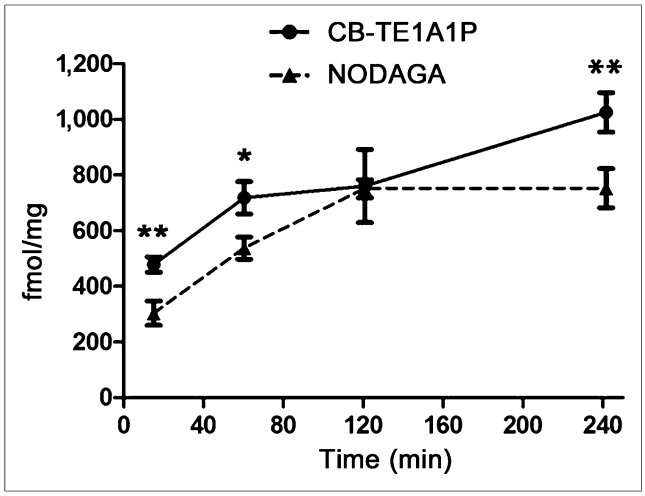


**FIGURE 2.** Internalization of $^{64}$Cu-CBTE1A1P-PEG$_4$-LLP2A and $^{64}$Cu-NODAGA-PEG$_4$-LLP2A (12 ng/well each) in B16F10 cells at 15 min and 1, 2, and 4 h. *$P < 0.05$. **$P < 0.01$.

tumor uptake (15.1 ± 1.0 and 14.0 ± 3.8 %ID/g, respectively); however, liver and kidney uptake were significantly lower for the CB-TE1A1P than for the NODAGA analog (liver: 3.0 ± 0.2 vs. 5.4 ± 0.6 %ID/g, $P < 0.001$; kidney: 2.9 ± 0.3 vs. 5.6 ± 0.9 %ID/g, $P < 0.001$). In addition, significantly higher tumor-to-blood and tumor-to-muscle ratios were observed for $^{64}$Cu-CB-TE1A1P-PEG$_4$-LLP2A than for $^{64}$Cu-NODAGA-PEG$_4$-LLP2A (tumor-to-blood: 17.9 ± 2.8 vs. 11.3 ± 3.1; tumor-to-muscle: 22.4 ± 1.3 vs. 18.1 ± 2.3; $P < 0.05$) (Figs. 3B and 3C). Blood clearance of the 2 radiopharmaceuticals was similar, with higher lung uptake for $^{64}$Cu-NODAGA-PEG$_4$-LLP2A (6.2 ± 0.7 vs. 4.6 ± 0.2; $P < 0.05$).

By 4 h after injection, the tumor uptake of $^{64}$Cu-CB-TE1A1P-PEG$_4$-LLP2A increased (16.9 ± 2.2 %ID/g), whereas it slightly decreased for $^{64}$Cu-NODAGA-PEG$_4$-LLP2A (13.4 ± 1.7 %ID/g). $^{64}$Cu-CB-TE1A1P-PEG$_4$-LLP2A cleared more efficiently from the blood; liver and kidney uptake remained lower than for $^{64}$Cu-NODAGA-PEG$_4$-LLP2A (liver: 2.4 ± 0.1 vs. 4.8 ± 0.3 %ID/g, $P < 0.0001$; kidney: 2.8 ± 0.5 vs. 4.3 ± 0.5 %ID/g, $P < 0.01$). The tumor-to-blood ratio was 46.3 ± 6.5 for $^{64}$Cu-CB-TE1A1P-PEG$_4$-LLP2A and 21.7 ± 3.3 for $^{64}$Cu-NODAGA-PEG$_4$-LLP2A ($P < 0.05$). Similarly, the tumor-to-muscle ratio was significantly higher for $^{64}$Cu-CB-TE1A1P-PEG$_4$-LLP2A than for $^{64}$Cu-NODAGA-PEG$_4$-LLP2A (28.9 ± 2.2 vs. 18.6 ± 0.3, respectively; $P < 0.01$). A separate blocking study was performed at 2 h after injection, in which agents were coadministered with excess LLP2A-PEG$_4$. The radiotracer uptake of both $^{64}$Cu-labeled agents was significantly reduced in the tumor, spleen, bone, and thymus, demonstrating specificity for VLA-4 in these tissues.

$^{68}$Ga-NODAGA-PEG$_4$-LLP2A (5.55 MBq, 37 MBq/μg) accumulated in the tumor up to 8.7 ± 1.3 %ID/g after 1 h and was cleared mainly by the kidney (7.0 ± 3.7 %ID/g); the liver uptake was 3.6 ± 1.3 %ID/g (Table 4). The $^{68}$Ga agent had good tumor-to-muscle and tumor-to-blood ratios (10.3 ± 1.5 and 4.4 ± 1.6, respectively) (Fig. 3A). Uptake was also observed in receptor-abundant organs such as the spleen, bone marrow, and thymus. In the presence of the blocking agent (excess LLP2A-PEG$_4$), the radiotracer uptake was significantly reduced in the VLA-4–positive tissues, demonstrating the targeting specificity of $^{68}$Ga-NODAGA-PEG$_4$-LLP2A.

### $^{68}$Ga Imaging in B16F10 Subcutaneous Tumor–Bearing Mice

High uptake of $^{68}$Ga-NODAGA-PEG$_4$-LLP2A was observed in the tumor with lower uptake in other receptor-rich organs such as the spleen and bone marrow; there was minimal uptake in the liver (Fig. 4). The radiopharmaceuticals cleared through the kidneys, and there was significant bladder activity, indicating rapid renal clearance. A reduction of the tumor uptake to background levels was observed with the blocking agent.

### $^{64}$Cu Imaging of B16F10 Subcutaneous Tumor

At 2 h after injection of $^{64}$Cu-NODAGA-PEG$_4$-LLP2A and $^{64}$Cu-CB-TE1A1P-PEG$_4$-LLP2A, the tumor was clearly visible (Fig. 5). After 4 and 24 h, the tumor was still visible in the mice

**TABLE 3**
Biodistribution of $^{64}$Cu-CB-TE1A1P-PEG$_4$-LLP2A and $^{64}$Cu-NODAGA-PEG$_4$-LLP2A in B16F10 Tumor–Bearing Mice

| Organs | $^{64}$Cu-NODAGA (2 h) | $^{64}$Cu-NODAGA (2-h block) | $^{64}$Cu-NODAGA (4 h) | $^{64}$Cu-CB-TE1A1P (2 h) | $^{64}$Cu-CB-TE1A1P (2-h block) | $^{64}$Cu-CB-TE1A1P (4 h) |
|---|---|---|---|---|---|---|
| Tumor | 14.0 ± 3.8 | 2.2 ± 0.7 | 13.4 ± 1.7 | 15.1 ± 1.0 | 0.9 ± 0.2 | 16.9 ± 2.2 |
| Thymus | 7.4 ± 2.6 | 0.6 ± 0.4 | 8.1 ± 1.2 | 6.5 ± 1.3 | 0.4 ± 0.1 | 7.1 ± 0.7 |
| Blood | 1.1 ± 0.5 | 0.6 ± 0.4 | 0.7 ± 0.2 | 1.2 ± 0.6 | 0.4 ± 0.3 | 0.4 ± 0.1 |
| Heart | 0.9 ± 0.1 | 0.9 ± 0.3 | 0.8 ± 0.1 | 0.6 ± 0.1 | 0.3 ± 0.1 | 0.4 ± 0.1 |
| Lung | 6.2 ± 0.7 | 3.6 ± 0.9 | 4.7 ± 0.6 | 4.6 ± 0.2 | 0.7 ± 0.2 | 3.9 ± 0.5 |
| Liver | 5.4 ± 0.6 | 6.8 ± 1.2 | 4.8 ± 0.3 | 3.0 ± 0.2 | 1.7 ± 0.3 | 2.4 ± 0.1 |
| Kidney | 5.6 ± 0.9 | 6.5 ± 1.7 | 4.3 ± 0.5 | 2.9 ± 0.2 | 2.9 ± 0.3 | 2.8 ± 0.5 |
| Spleen | 23.9 ± 4.8 | 0.7 ± 0.5 | 15.6 ± 5.1 | 18.1 ± 1.3 | 0.3 ± 0.1 | 15.3 ± 2.1 |
| Muscle | 1.0 ± 0.3 | 0.2 ± 0.2 | 0.7 ± 0.1 | 1.3 ± 0.8 | 0.2 ± 0.1 | 0.8 ± 0.3 |
| Bone | 6.1 ± 1.8 | 0.8 ± 0.5 | 3.9 ± 0.1 | 7.9 ± 1.9 | 0.9 ± 0.5 | 7.7 ± 1.2 |
| Small intestine | 5.2 ± 1.8 | 6.7 ± 2.7 | 4.3 ± 1.5 | 2.6 ± 1.0 | 0.9 ± 0.5 | 2.1 ± 0.2 |
| Large intestine | 4.3 ± 3.1 | 2.7 ± 0.9 | 7.9 ± 1.1 | 1.4 ± 0.3 | 0.3 ± 0.1 | 1.2 ± 0.7 |

$n = 4$; values are expressed as mean ± SD.

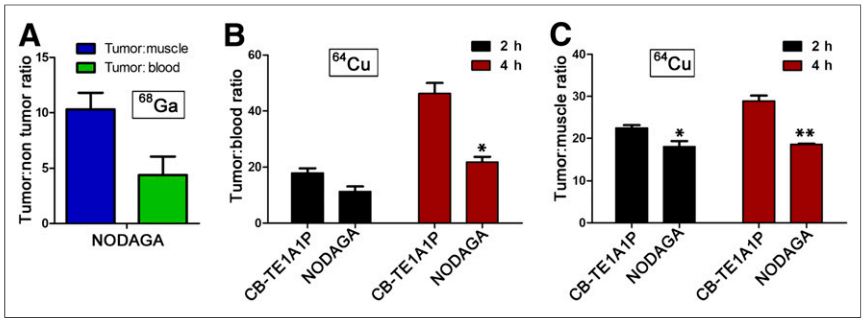


**FIGURE 3.** (A) Tumor-to-blood and tumor-to-muscle ratios of $^{68}$Ga-NODAGA-PEG$_4$-LLP2A. Comparison of tumor-to-blood (B) and tumor-to-muscle (C) ratios of $^{64}$Cu-NODAGA-PEG$_4$-LLP2A and $^{64}$Cu-CB-TE1A1P-PEG$_4$-LLP2A. $^*P < 0.05$. $^{**}P < 0.01$.

injected with $^{64}$Cu-CB-TE1A1P-PEG$_4$-LLP2A, whereas in mice injected with the NODAGA analog the tumor signal and visibility decreased significantly. $^{64}$Cu-CB-TE1A1P-PEG$_4$-LLP2A showed higher tumor uptake (Fig. 5C) and tumor-to-muscle ratios (Fig. 5D) than $^{64}$Cu-NODAGA-PEG$_4$-LLP2A at all time points. In addition, the tumor-to-muscle ratio increased at 4 and 24 h, compared with 2 h, for the $^{64}$Cu-CB-TE1A1P-PEG$_4$-LLP2A, whereas the tumor-to-muscle ratio for $^{64}$Cu-NODAGA-PEG$_4$-LLP2A increased at 4 h and decreased at 24 h. Blocking reduced tumor uptake for both agents.

### Imaging of Metastatic B16F10 Melanoma

Malignant melanoma has a high likelihood of metastasizing to regional lymph nodes and distant organs. To determine how well the LLP2A agents imaged small metastases, we evaluated $^{68}$Ga-NODAGA-PEG$_4$-LLP2A and $^{64}$Cu-CB-TE1A1P-PEG$_4$-LLP2A conjugates in a mouse metastatic melanoma model. B16F10 melanoma cells were transfected with luciferase, which allows imaging of metastatic sites as they develop. Albino C57BL/6 mice were injected in the left ventricle with B16F10_Luc_tdT cells and monitored for metastasis over 3 wk. These mice developed invasive metastases in the lungs, bone marrow, ovaries, lymph nodes, adrenal glands, and heart. Mice were dissected after imaging to confirm sites of metastasis. Bioluminescence imaging was performed the same day as PET/CT imaging, before injection of the radiopharmaceuticals.

PET/CT imaging with $^{64}$Cu-CB-TE1A1P-PEG$_4$-LLP2A was performed 2 h after injection (Fig. 6). The probe was able to detect lung, bone (metastasis size, 1–2 mm), adrenal gland, ovaries, and lymph node metastases. The uptake correlated with the bioluminescence images of the tumor cells (Fig. 6A) as well as with the metastatic lesions identified by CT (Supplemental Figs. 5B and 5C).

$^{68}$Ga-NODAGA-PEG$_4$-LLP2A detected small metastases in the lungs and bones (metastasis size, 1–2 mm) at 1 h (Fig. 7). The uptake of the probe correlated with the bioluminescence images of tumor metastases (Fig. 7A). In addition, the uptake in the lungs correlated with metastases as identified by CT (Supplemental Fig. 6B). $^{68}$Ga-NODAGA-PEG$_4$-LLP2A also had high uptake in the ovaries that was due to the presence of metastasis not visible by bioluminescence imaging, likely due to its lower sensitivity.

## DISCUSSION

Metastatic melanoma is an aggressive type of cancer with no proven long-term effective therapy and a low survival rate. Melanoma cells express a wide range of integrins, including $\alpha_v\beta_3$, $\alpha_2\beta_1$, $\alpha_3\beta_1$, and $\alpha_4\beta_1$ (or VLA-4) (*19*), and upregulation of VLA-4 in melanoma is associated with a more metastatic phenotype (*15–18*). VLA-4 is an adhesion molecule involved in cancer cell trafficking and metastasis by promoting adhesion to endothelial cells and favoring transendothelial migration (*24*). The expression of VLA-4 on primary

**TABLE 4**
Biodistribution of $^{68}$Ga-NODAGA-PEG$_4$-LLP2A in B16F10 Tumor–Bearing Mice

| Organs | $^{68}$Ga-NODAGA (1 h) | $^{68}$Ga-NODAGA (1-h block) |
|---|---|---|
| Tumor | 8.7 ± 1.3 | 1.6 ± 0.5 |
| Thymus | 6.1 ± 1.2 | 0.5 ± 0.3 |
| Blood | 2.3 ± 1.1 | 1.5 ± 1.1 |
| Heart | 1.1 ± 0.4 | 0.7 ± 0.4 |
| Lung | 3.9 ± 1.1 | 1.4 ± 0.4 |
| Liver | 3.6 ± 1.3 | 2.6 ± 0.6 |
| Kidney | 7.0 ± 3.7 | 4.5 ± 1.1 |
| Spleen | 11.9 ± 1.5 | 0.6 ± 0.2 |
| Muscle | 1.2 ± 0.8 | 0.3 ± 0.1 |
| Bone | 3.6 ± 0.9 | 0.6 ± 0.2 |
| Small intestine | 3.5 ± 1.9 | 2.7 ± 1.9 |
| Large intestine | 1.0 ± 0.2 | 0.3 ± 0.1 |

$n = 4$; values are expressed as mean ± SD.

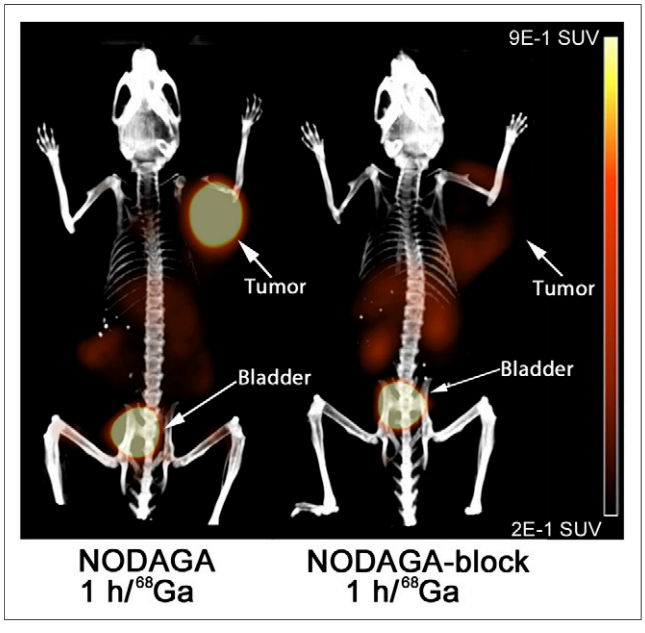


**FIGURE 4.** Small-animal PET/CT imaging with $^{68}$Ga-NODAGA-PEG$_4$-LLP2A (7.4 MBq, 370 ng) in B16F10 tumor–bearing mice at 1 h after injection, with or without excess LLP2A-PEG$_4$ as a blocking agent.

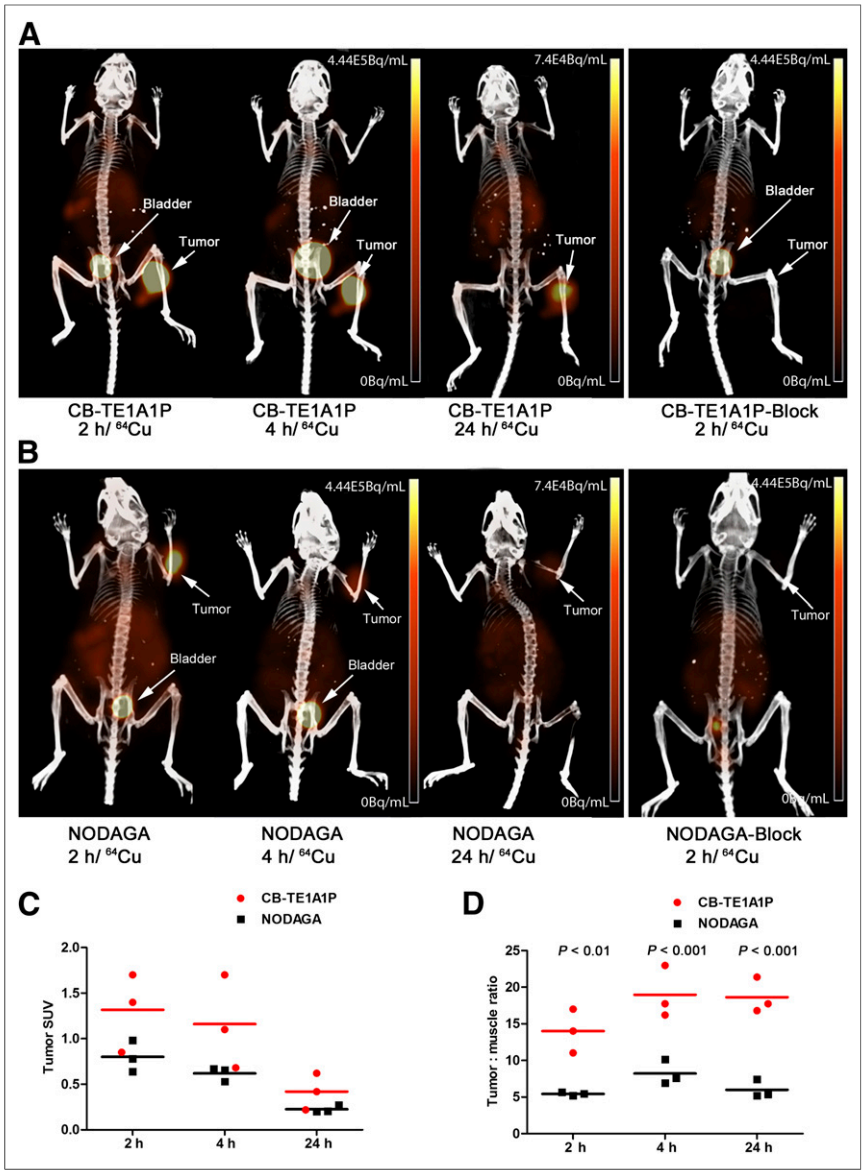


**FIGURE 5.** Small-animal PET/CT imaging of B16F10 tumor–bearing mice at 2, 4, and 24 h after injection of $^{64}$Cu-CB-TE1A1P-PEG$_4$-LLP2A (A) or $^{64}$Cu-NODAGA-PEG$_4$-LLP2A (B), with or without coinjection of excess LLP2A-PEG$_4$ as blocking agent. (C) Mean SUVs of tumor were calculated by drawing ROIs on total volume of tumor ($n$ = 3 mice per compound). (D) Tumor-to-muscle ratios were calculated by dividing mean tumor SUV over mean muscle SUV (muscle SUV was calculated by drawing cylinder ROI on gastrocnemius muscle) ($n$ = 3 mice per compound).

melanomas correlates with the development of metastasis (*18*) and has been associated with a high risk of metastasis and tumor progression (*15,16*). Thus, a sensitive and noninvasive imaging probe will be highly desirable to evaluate the expression of activated VLA-4 on melanoma to specifically image metastatic potential of this type of cancer.

We previously showed that the CB-TE1A1P was superior to CB-TE2A as a chelator for LLP2A (*22*). Here, we investigated attaching the NODAGA chelator due to its ability to stably incorporate both $^{64}$Cu and $^{68}$Ga. We also replaced the double linker 4-((2-(2-(2-aminoethoxy)ethoxy)ethyl)amino)-4-oxobutanoic acid with a polyethylenglycol (PEG-4) linker, which increased the binding affinity of the CB-TE1A1P-LLP2A conjugate by 5-fold, probably because of the improvement of the water solubility of the compound.

The $^{64}$Cu conjugates were evaluated in vitro by saturation binding and internalization assays using B16F10 cells. NODAGA-PEG$_4$-LLP2A and CB-TE1A1P-PEG$_4$-LLP2A showed similar binding affinity (0.23 ± 0.03 and 0.28 ± 0.03 nM, respectively), but the CB-TE1A1P conjugate bound more receptor sites ($B_{max}$, 296 ± 4.5 fmol/mg) than the NODAGA conjugate ($B_{max}$, 243 ± 5.2 fmol/mg). The $^{64}$Cu-CB-TE1A1P conjugate accumulated in B16F10 cells out to 4 h, whereas uptake of the $^{64}$Cu-NODAGA conjugate plateaued at 2 h. The efflux data did not show any difference between the 2 compounds (Supplemental Fig. 3), indicating that the decreased cell accumulation for the NODAGA compound is not related to the efflux of the compound. The net charge of CB-TE1A1P-PEG$_4$-LLP2A is −1, compared with a charge of −2 for NODAGA-PEG$_4$-LLP2A. The increased negative charge may induce more repulsion with the cell membrane and may interfere with the binding and internalization of the LLP2A conjugate.

The in vivo data show clear superiority of the $^{64}$Cu-CB-TE1A1P-PEG$_4$-LLP2A, compared with $^{64}$Cu-NODAGA-PEG$_4$-LLP2A, with higher tumor uptake, significantly lower liver and kidney uptake, and significantly higher tumor-to-muscle and tumor-to-blood ratios of the CB-TE1A1P versus the NODAGA conjugate. In addition, the CB-TE1A1P agent showed greater affinity to plasma proteins, which may improve its circulation in the blood and result in higher tumor uptake. PET/CT imaging in subcutaneous B16F10 tumors validated that $^{64}$Cu-CB-TE1A1P-PEG$_4$-LLP2A is the optimal imaging compound, especially at longer time points. The images showed excellent tumor contrast for both compounds at 2 h, and although the contrast started to decrease for the NODAGA conjugate at 4 and 24 h, the tumor was clearly visible with the CB-TE1A1P agent. Image quantification data confirm the superior performance of the CB-TE1A1P conjugate.

To our knowledge, this is the first report of a $^{68}$Ga-labeled LLP2A conjugate. Here, we show that $^{68}$Ga-NODAGA-PEG$_4$-LLP2A binds with high affinity to VLA-4 ($K_i$ = 0.11 nM) and images melanoma and melanoma metastases in a mouse model with high contrast. The biodistribution data showed that $^{68}$Ga-NODAGA-PEG$_4$-LLP2A has high and specific uptake in the B16F10 melanoma tumor as early as 1 h after injection (8.7 ± 1.3 %ID/g). $^{68}$Ga-NODAGA-PEG$_4$-LLP2A was mainly cleared through the kidneys with relatively low liver uptake and had good tumor-to-muscle (10.3 ± 1.5) and tumor-to-blood (4.4 ± 1.6) ratios. The small-animal PET/CT images clearly show the tumor and other VLA-4–rich organs.

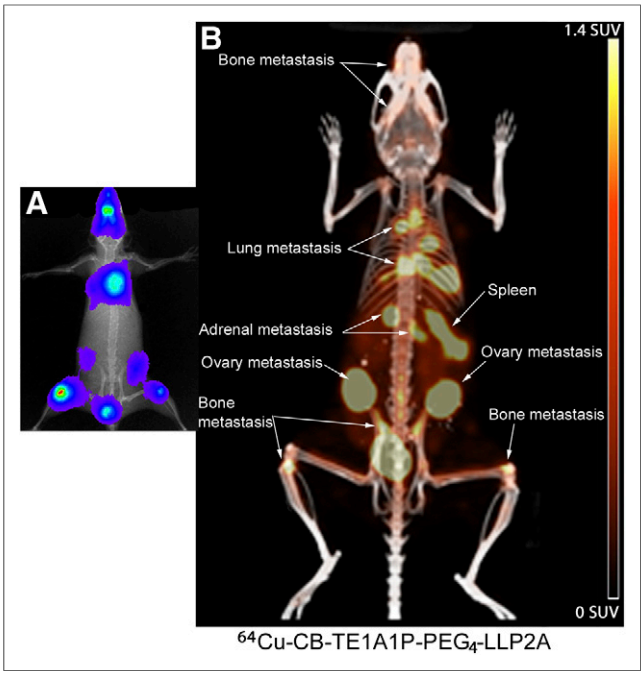


**FIGURE 6.** (A) Bioluminescence images showing the sites of metastasis. (B) Small-animal PET/CT imaging of $^{64}$Cu-CB-TE1A1P-PEG$_4$-LLP2A in B16F10_Luc_tdT metastases at 2 h after injection (7.4 MBq).

Melanoma is known to metastasize to distant sites, and imaging of small metastases is challenging. Here, we demonstrate 2 new tracers, $^{64}$Cu-CB-TE1A1P-PEG$_4$-LLP2A and $^{68}$Ga-NODAGA-PEG$_4$-LLP2A, that have high uptake in B16F10 metastases with high contrast. The B16F10 melanoma cell line was transfected successfully with luciferase, and the tumor metastasis was readily monitored by bioluminescence imaging. Flow cytometry analysis indicates that the transfection did not affect the expression of VLA-4 or the affinity of LLP2A to the receptor (Supplemental Fig. 2).

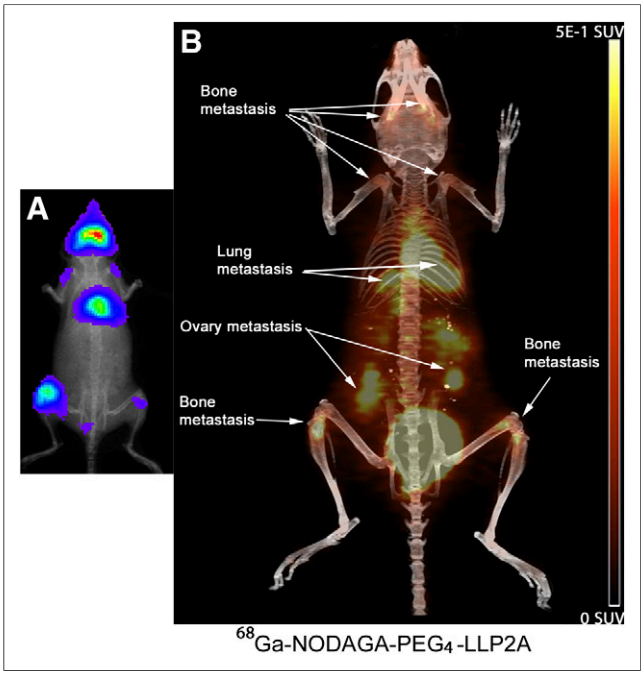


**FIGURE 7.** (A) Bioluminescence images showing the sites of metastasis. (B) Small-animal PET/CT images of $^{68}$Ga-NODAGA-PEG$_4$-LLP2A in B16F10_Luc_tdT metastases at 1 h after injection (6.5 MBq).

$^{18}$F-FDG is currently used for imaging and staging melanoma but has limitations, especially for imaging small metastases, for which it appeared to be less sensitive (*7*). In the case of lung metastases, the high heart uptake of $^{18}$F-FDG can interfere in delineating lung lesions. Ren et al. (*9*) investigated melanin-targeted $^{18}$F-FBZA for specific imaging of melanoma and showed that lung uptake was significantly higher in murine lungs bearing melanotic B16F10 pulmonary metastases than in normal murine lungs, without specifically showing uptake in focal metastatic lesions. $^{64}$Cu-CB-TE1A1P-PEG$_4$-LLP2A and $^{68}$Ga-NODAGA-PEG$_4$-LLP2A were able to image melanoma lung metastases with high contrast and minimal lung background (Figs. 6 and 7). In addition, we were able to image small metastases in bone with high sensitivity. Guo et al. (*10*) imaged melanoma lung metastases by targeting the melanocortin receptor-1 with $^{67}$Ga-DOTA-GlyGlu-CycMSH; however, they reported high kidney uptake that can limit the detection of metastases near the kidneys. LLP2A conjugates are not retained in the kidneys, and $^{64}$Cu-CB-TE1A1P-PEG$_4$-LLP2A easily visualized adrenal metastases. Furthermore, $^{64}$Cu-CB-TE1A1P-PEG$_4$-LLP2A and $^{68}$Ga-NODAGA-PEG$_4$-LLP2A were able to image metastases in lymph nodes and ovaries.

Increased expression of VLA-4 has been reported to correlate with an aggressive and highly metastatic profile of melanoma. The presence of VLA-4 in only the high-affinity/avidity state leads to transendothelial migration across vascular cell adhesion molecule-1 and metastasis in melanoma (*25*). Therefore, LLP2A conjugates may provide a unique and noninvasive method of characterizing the biologic aggressiveness of melanoma via specific imaging of the high-affinity state of the VLA-4 receptor. This can be of great importance, because to the best of our knowledge, $^{18}$F-FDG has not demonstrated differential uptake in primary-only versus metastatic primary melanoma. Histology on tissue biopsy using anti–VLA-4 or anti-$\alpha_4$ antibodies will provide only information on the presence of the VLA-4 receptor in either the active or the inactive form and not specifically the high-affinity/avidity state.

## CONCLUSION

Here, we compared $^{64}$Cu-labeled NODAGA- and CB-TE1A1P-PEG$_4$-LLP2A conjugates and evaluated $^{68}$Ga-labeled NODAGA-PEG$_4$-LLP2A for imaging mouse models of primary and metastatic melanoma. Our results show that all 3 compounds are excellent imaging agents, with $^{64}$Cu-CB-TE1A1P-PEG$_4$-LLP2A being superior with higher tumor uptake and lower kidney and liver uptake. These new VLA-4–targeting agents are able to detect small melanoma metastases and may have advantages over imaging metastatic melanoma with $^{18}$F-FDG, because high levels of activated VLA-4 indicate an aggressive state of melanoma.

## DISCLOSURE

The costs of publication of this article were defrayed in part by payment of page charges. Therefore, and solely to indicate this fact, this article is hereby marked “advertisement” in accordance with 18 USC section 1734. This research was supported in part by NIH NCI 1R21CA180211. Small-animal PET/CT imaging at the In Vivo Imaging Facility at UPCI was supported in part by P30CA047904 (UPCI CCSG). No other potential conflicts of interest relevant to this article are reported.

## ACKNOWLEDGMENTS

We are grateful to Kathryn Day and Joseph Latoche for maintaining the preclinical PET/CT imaging facility and Meltem Ocak for helpful discussions.

## REFERENCES

1. Patel JK, Didolkar MS, Pickren JW, Moore RH. Metastatic pattern of malignant melanoma: a study of 216 autopsy cases. *Am J Surg.* 1978;135:807–810.
2. Markovic SN, Erickson LA, Rao RD, et al. Malignant melanoma in the 21st century, part 1: epidemiology, risk factors, screening, prevention, and diagnosis. *Mayo Clin Proc.* 2007;82:364–380.
3. Rose PG. Re: annual report to the nation on the status of cancer (1973 through 1998), featuring cancer with recent increasing trends. *J Natl Cancer Inst.* 2001;93:1656.
4. Balch CM, Gershenwald JE, Soong SJ, et al. Final version of 2009 AJCC melanoma staging and classification. *J Clin Oncol.* 2009;27:6199–6206.
5. Chapman PB, Hauschild A, Robert C, et al. Improved survival with vemurafenib in melanoma with BRAF V600E mutation. *N Engl J Med.* 2011;364:2507–2516.
6. Villanueva J, Vultur A, Herlyn M. Resistance to BRAF inhibitors: unraveling mechanisms and future treatment options. *Cancer Res.* 2011;71:7137–7140.
7. Prichard RS, Hill AD, Skehan SJ, O'Higgins NJ. Positron emission tomography for staging and management of malignant melanoma. *Br J Surg.* 2002;89:389–396.
8. Choi EA, Gershenwald JE. Imaging studies in patients with melanoma. *Surg Oncol Clin N Am.* 2007;16:403–430.
9. Ren G, Miao Z, Liu H, et al. Melanin-targeted preclinical PET imaging of melanoma metastasis. *J Nucl Med.* 2009;50:1692–1699.
10. Guo H, Yang J, Shenoy N, Miao Y. Gallium-67-labeled lactam bridge-cyclized α-melanocyte stimulating hormone peptide for primary and metastatic melanoma imaging. *Bioconjug Chem.* 2009;20:2356–2363.
11. Beer AJ, Haubner R, Goebel M, et al. Biodistribution and pharmacokinetics of the αvβ3-selective tracer $^{18}$F-galacto-RGD in cancer patients. *J Nucl Med.* 2005;46:1333–1341.
12. Miyake K, Hasunuma Y, Yagita H, Kimoto M. Requirement for VLA-4 and VLA-5 integrins in lymphoma cells binding to and migration beneath stromal cells in culture. *J Cell Biol.* 1992;119:653–662.
13. Juneja HS, Schmalsteig FC, Lee S, Chen J. Vascular cell adhesion molecule-1 and VLA-4 are obligatory adhesion proteins in the heterotypic adherence between human leukemia/lymphoma cells and marrow stromal cells. *Exp Hematol.* 1993;21:444–450.
14. Holzmann B, Gosslar U, Bittner M. α4 integrins and tumor metastasis. *Curr Top Microbiol Immunol.* 1998;231:125–141.
15. Hart IR, Birch M, Marshall JF. Cell adhesion receptor expression during melanoma progression and metastasis. *Cancer Metastasis Rev.* 1991;10:115–128.
16. Moretti S, Martini L, Berti E, Pinzi C, Giannotti B. Adhesion molecule profile and malignancy of melanocytic lesions. *Melanoma Res.* 1993;3:235–239.
17. Schadendorf D, Heidel J, Gawlik C, Suter L, Czarnetzki BM. Association with clinical outcome of expression of VLA-4 in primary cutaneous malignant melanoma as well as P-selectin and E-selectin on intratumoral vessels. *J Natl Cancer Inst.* 1995;87:366–371.
18. Schadendorf D, Gawlik C, Haney U, Ostmeier H, Suter L, Czarnetzki BM. Tumour progression and metastatic behaviour in vivo correlates with integrin expression on melanocytic tumours. *J Pathol.* 1993;170:429–434.
19. Kuphal S, Bauer R, Bosserhoff AK. Integrin signaling in malignant melanoma. *Cancer Metastasis Rev.* 2005;24:195–222.
20. Peng L, Liu R, Marik J, Wang X, Takada Y, Lam KS. Combinatorial chemistry identifies high-affinity peptidomimetics against α4β1 integrin for in vivo tumor imaging. *Nat Chem Biol.* 2006;2:381–389.
21. Shokeen M, Zheleznyak A, Wilson JM, et al. Molecular imaging of very late antigen-4 ($\alpha_4\beta_1$ integrin) in the premetastatic niche. *J Nucl Med.* 2012;53:779–786.
22. Jiang M, Ferdani R, Shokeen M, Anderson CJ. Comparison of two cross-bridged macrocyclic chelators for the evaluation of $^{64}$Cu-labeled-LLP2A, a peptidomimetic ligand targeting VLA-4-positive tumors. *Nucl Med Biol.* 2013;40:245–251.
23. Soodgupta D, Hurchla MA, Jiang M, et al. Very late antigen-4 ($\alpha_4\beta_1$ integrin) targeted PET imaging of multiple myeloma. *PLoS ONE.* 2013;8:e55841.
24. Hauzenberger D, Klominek J, Holgersson J, Bergstrom SE, Sundqvist KG. Triggering of motile behavior in T lymphocytes via cross-linking of alpha 4 beta 1 and alpha L beta 2. *J Immunol.* 1997;158:76–84.
25. Klemke M, Weschenfelder T, Konstandin MH, Samstag Y. High affinity interaction of integrin alpha4beta1 (VLA-4) and vascular cell adhesion molecule 1 (VCAM-1) enhances migration of human melanoma cells across activated endothelial cell layers. *J Cell Physiol.* 2007;212:368–374.

The Journal of NUCLEAR MEDICINE

# PET Imaging of Very Late Antigen-4 in Melanoma: Comparison of $^{68}$Ga- and $^{64}$Cu-Labeled NODAGA and CB-TE1A1P-LLP2A Conjugates

Wissam Beaino and Carolyn J. Anderson

*J Nucl Med.* 2014;55:1856-1863.
Published online: September 25, 2014.
Doi: 10.2967/jnumed.114.144881



*The Journal of Nuclear Medicine* is published monthly.
SNMMI | Society of Nuclear Medicine and Molecular Imaging
1850 Samuel Morse Drive, Reston, VA 20190.
(Print ISSN: 0161-5505, Online ISSN: 2159-662X)



SNMMI SOCIETY OF NUCLEAR MEDICINE AND MOLECULAR IMAGING